

continuous monitoring of the heliosphere with ground-based radio telescopes could substantially supplement future spacecraft observations, thus suggesting a future synergistic approach to ground- and space-based observations.

REFERENCES AND NOTES

1. A. Wolszczan, *Science* **264**, 538 (1994).
2. R. Malhotra, *Astrophys. J.* **407**, 266 (1993); F. A. Rasio, P. D. Nicholson, S. L. Shapiro, S. A. Teukolsky, in *Planets Around Pulsars*, J. A. Phillips, J. E. Thorsett, S. R. Kulkarni, Eds. (ASP Conf. Ser. 36, Astronomical Society of the Pacific, San Francisco, CA, 1993), pp. 107–119.
3. K. Scherer and J. D. Anderson, *Eos (Fall Suppl.)* **76**, F332 (1995).
4. D. F. Gray, *Nature* **385**, 795 (1997).
5. The experiment was designed as a celestial mechanics experiment to measure masses, special relativity effects, and recently, to detect large objects in the Edgeworth-Kuiper Belt.
6. The Doppler data are coherently referenced to hydrogen-maser frequency standards at Deep Space Network (DSN) stations in California, Australia, and Spain, and the radio wave transmitted from the ground is transponded by the spacecraft's telecommunication subsystem with a frequency ratio of 240/221. A summary of the Pioneer telecommunication subsystem, as well as other aspects of the spacecraft and its mission, can be found in R. O. Fimmel, J. Van Allen, and E. Burgess [*Pioneer: First to Jupiter, Saturn, and Beyond*, NASA SP-446 (Government Printing Office, Washington, DC, 1980)]. For a discussion of nonlinear least squares applied specifically to spacecraft orbit determination, see T. D. Moyer [*Mathematical Formulation of the Double Precision Orbit Determination Program* (JPL TR 32-1527, Jet Propulsion Laboratory, Pasadena, CA, 1971)], B. D. Tapley [in *Recent Advances in Dynamical Astronomy*, B. D. Tapley and V. Szebehely, Eds. (Reidel, Boston, MA, 1973), pp. 396–425], and J. D. Anderson [in *Experimental Gravitation*, B. Bertotti, Ed. (Academic Press, New York, 1974), pp. 163–199].
7. K. Mursula and B. J. Zieger, *J. Geophys. Res.* **101**, 27077 (1996).
8. J. D. Richardson, K. I. Paularena, J. W. Belcher, A. J. Lazarus, *Geophys. Res. Lett.* **21**, 1559 (1994).
9. The solar wind data can be found at the following Web sites. Ames Research Center Pioneer Plasma Group home page: <http://arwen.arc.nasa.gov>; National Space Science Data Center (NSSDC) COHWeb: http://nssdc.gsfc.nasa.gov/cohweb/form/cw_ds.html; NSSDC OMNIWeb: <http://nssdc.gsfc.nasa.gov/omniweb/ow.html>
10. The data do not cover a full year because during conjunction the radio ray path passes the sun at about 11 solar radii, which is very close to the formation region of the solar wind in the ecliptic. Therefore turbulent plasma processes are dominant, and the radio signal to P10 is noisy.
11. R. von Steiger, J. Geiss, G. Gloeckler, A. B. Galvin, *Space. Sci. Rev.* **72**, 71 (1995); L. F. Burlaga, *J. Geophys. Res.* **93**, 4103 (1988); J. L. Phillips *et al.*, *Science* **268**, 1030 (1995).
12. M. K. Bird, *Space. Sci. Rev.* **33**, 99 (1982).
13. With a pulsar mass m_{PSR} of 1.4 solar masses, a planetary mass m_{C} of 0.015 Earth masses, and the planetary semimajor axis $a_{\text{C}} = 0.19$ AU, it follows from $a_{\text{PSR}} = a_{\text{C}} m_{\text{C}} / m_{\text{PSR}} = 0.19$ km.
14. D. O. Muhleman and J. D. Anderson, *Astrophys. J.* **247**, 1093 (1981).
15. A possible third object with a revolution period of about 170 years was recently reported [A. Wolszczan, in *Pulsars: Problems and Progress*, M. Bailes, S. Johnston, M. Walker, Eds., *IAU Colloquium* **160**, 91 (1996)].
16. M. K. Bird, in *Solar Wind 4*, H. Rosenbauer, Ed. (Report MPAE-W-100-81-31, Max-Planck-Institut für Aeronomie, Katlenburg-Lindau, Germany, 1981), pp. 78–83.

17. Part of this work was sponsored by the Pioneer Project, NASA Ames Research Center and was performed at the Jet Propulsion Laboratory (JPL), California Institute of Technology, under contract with NASA. The Pioneer 10 radio Doppler data were gen-

erated with the support of JPL's Telecommunications and Mission Operations Directorate and the DSN.

14 August 1997; accepted 30 October 1997

Radar Detection of the Nucleus and Coma of Comet Hyakutake (C/1996 B2)

J. K. Harmon,* S. J. Ostro, L. A. M. Benner, K. D. Rosema, R. F. Jurgens, R. Winkler, D. K. Yeomans, D. Choate, R. Cormier, J. D. Giorgini, D. L. Mitchell,† P. W. Chodas, R. Rose, D. Kelley, M. A. Slade, M. L. Thomas

Radar observations of comet Hyakutake (C/1996 B2) made at the Goldstone Deep Space Communications Complex in California have detected echoes from the nucleus and from large grains in the inner coma. The nucleus of this bright comet was estimated to be only 2 to 3 kilometers in diameter. Models of the coma echo indicate backscatter from porous, centimeter-size grains ejected anisotropically at velocities of tens of meters per second. The radar observations suggest that a comet's activity may be a poor indicator of its size and provide evidence that large grains constitute an important component of the mass loss from a typical active comet.

Radar is one of the most powerful Earth-based techniques for studying comets because it can be used to directly probe the nucleus as well as identify populations of large grains in the coma. Unfortunately, comet radar detections are rare events, because few of these small objects pass close enough to Earth to give measurable echoes. Before Hyakutake only five comets had yielded radar detections. Three of these detections [P/Encke (1), P/Grigg-Skjellerup (2), and C/Sugano-Saigusa-Fujikawa 1983 J1 (3)] were of the nucleus alone. Comet C/IRAS-Araki-Alcock 1983 H1 (henceforth referred to as IAA) made the closest approach [0.031 astronomical unit (AU)] of the five and also was the first to show echoes from large coma grains as well as from the nucleus (4, 5). The 1985 apparition of comet P/Halley produced the last and most distant (0.63 AU) comet radar detection; Halley showed only a coma echo, the nucleus echo being too weak to be seen at this distance (6). Comet Hyakutake (C/1996 B2), which passed within 0.10 AU of Earth, offered the first good comet radar opportunity in 13 years and the first chance

to observe a bright comet at close range.

Radar observations of Hyakutake were made in March 1996 with the X-band (8510 MHz; wavelength, λ , of 3.5 cm) radar on the 70-m antenna at the Goldstone facility in California. Echo detections were obtained on 24 and 25 March, when the comet was near its closest approach distance (Fig. 1). As with previous comet detections, the Hyakutake detections were made with an unmodulated continuous-wave (CW) transmission (7). A 490-kW, circularly polarized wave was transmitted, and the echoes were received in the opposite-sense circular (OC) and same-sense circular (SC) polarizations (8). The received signal was sampled and analyzed to give calibrated (9) echo power spectra with frequency resolutions of either 19.5 Hz (low resolution) or 1.95 Hz (high resolution). The spectra were summed for each polarization to give one low-resolution and one high-resolution spectrum pair for 24 March, and one low-resolution spectrum pair for 25 March.

Both low-resolution spectra (Fig. 2, A and B) from the two successive days show a narrow spike, which is the nucleus echo, along with a broad hump skewed toward the negative side of the spike, which is the coma echo. The nucleus echo can also be seen at 210 Hz in the high-resolution spectrum (Fig. 2C). (The total bandwidth of this spectrum was too narrow to recover the full coma echo, and we have subtracted any residual coma echo left after noise baseline removal.) Integrating under the three nucleus echoes in Fig. 2 gives total radar cross

J. K. Harmon, National Astronomy and Ionosphere Center, Arecibo Observatory, Post Office Box 995, Arecibo, PR 00614, USA.

S. J. Ostro, L. A. M. Benner, K. D. Rosema, R. F. Jurgens, R. Winkler, D. K. Yeomans, D. Choate, R. Cormier, J. D. Giorgini, D. L. Mitchell, P. W. Chodas, R. Rose, D. Kelley, M. A. Slade, M. L. Thomas, Jet Propulsion Laboratory, California Institute of Technology, 4800 Oak Grove Drive, Pasadena, CA 91109-8099, USA.

*To whom correspondence should be addressed.

†Present address: Space Sciences Laboratory, University of California, Berkeley, CA 94720, USA.

sections $\sigma = \sigma_{oc} + \sigma_{sc}$ of 0.187 km^2 , 0.192 km^2 , and 0.178 km^2 , respectively, with $\pm 30\%$ uncertainty (10). The nucleus polarization ratio $\mu_c \equiv \sigma_{sc}/\sigma_{oc}$ ranges from 0.39 to 0.70 for the three spectral pairs and averages 0.49, indicating that Hyakutake's decimeter-scale surface roughness is comparable with that of the rougher near-Earth asteroids (11). Because this comet is very active for its size, it is possible that the high roughness is associated with sublimation erosion or fallback of ejected debris (12).

We estimate the OC cross sections for the coma echo to be 1.25 km^2 and 1.42 km^2 from Fig. 2, A and B, respectively (with $\pm 30\%$ uncertainty). This makes the coma echo an order of magnitude stronger than the nucleus echo. The SC coma echo is weaker than the OC coma echo. This $\mu_c < 1$ behavior was also seen in the coma echoes from IAA (5) and Halley (6) and is consistent with single scattering from coma grains (8).

Attempts to make a range-resolved detection (7) of Hyakutake failed, so we were not able to measure the nucleus size directly.

However, we can estimate the size of the nucleus from its radar cross section and Doppler spread. The total cross section of 0.19 km^2 of the Hyakutake nucleus is the second smallest of the five comets that have yielded nucleus detections (13). This implies that Hyakutake, unless it has an abnormally low radar albedo, must be a relatively small comet. Probably the most reliable estimate for the radar albedo of a comet nucleus is the 0.039 value estimated for comet IAA (14), which corresponds to a surface with the consistency of packed snow or very loose soil (5). If we assume an albedo of 0.039, we calculate a diameter of 2.5 km for Hyakutake's nucleus (Fig. 3). This small diameter is consistent with the small Doppler bandwidth of the nucleus echo. The diameter of a nucleus with a rotation period P , in hours, and a rotational Doppler bandwidth (at $\lambda = 3.5 \text{ cm}$) of B , in hertz, is given by $D = (1.0 \times 10^{-2})BP/\sin i$, where i is the angle between the line of sight and the rotation axis. We obtained an estimate of $B = 12 \pm 4 \text{ Hz}$ by fitting the high-resolution OC spectrum with a model nucleus echo

computed from the convolution of a $\cos^{3/2} \theta$ scattering law with the -15 Hz per hour ephemeris drift (Fig. 2C). From optical observations of coma variability and dust jet rotation, the rotation period P of Hyakutake's nucleus has been estimated to be either 6.25 hours (15) or 12.5 hours (16). Combining these B and P values gives lower limits of 0.75 or 1.5 km for the nucleus diameter for $P = 6.25$ hours and $P = 12.5$ hours, respectively (Fig. 3). Therefore, we conclude that Hyakutake is a much smaller comet than either IAA (14) or Halley (17). This is consistent with estimates and upper limits for the size of Hyakutake's nucleus based on infrared and radio continuum observations (18). A small nucleus can also be inferred from the behavior of this comet's orbital motion. Hyakutake is one of the few long-period comets for which the inclusion of a nongravitational outgassing acceleration model was necessary to represent properly the optical and radar Doppler observations (19). Apparently, Hyakutake's small mass allows it to be pushed around by its active jets with relative ease.

The broadband component of the echo represents backscatter by large grains ejected from the nucleus at speeds of tens of meters per second. These grains can be anywhere within the 7000-km-diameter cylinder subtended by the radar beam at the comet, a region that includes much of the so-called "inner coma." The coma echo is asymmetric, with most of the echo offset to the negative-Doppler side of the nucleus. This asymmetry implies an anisotropy in the direction of grain ejection. We evaluated possible grain ejection geometries and velocities using the approach of Harmon *et al.* (5) to the IAA coma echo. We assumed that the grains had an $a^{-3.9}$ production size distribution, where a is grain radius, and that they were ejected in a 90° -wide cone at

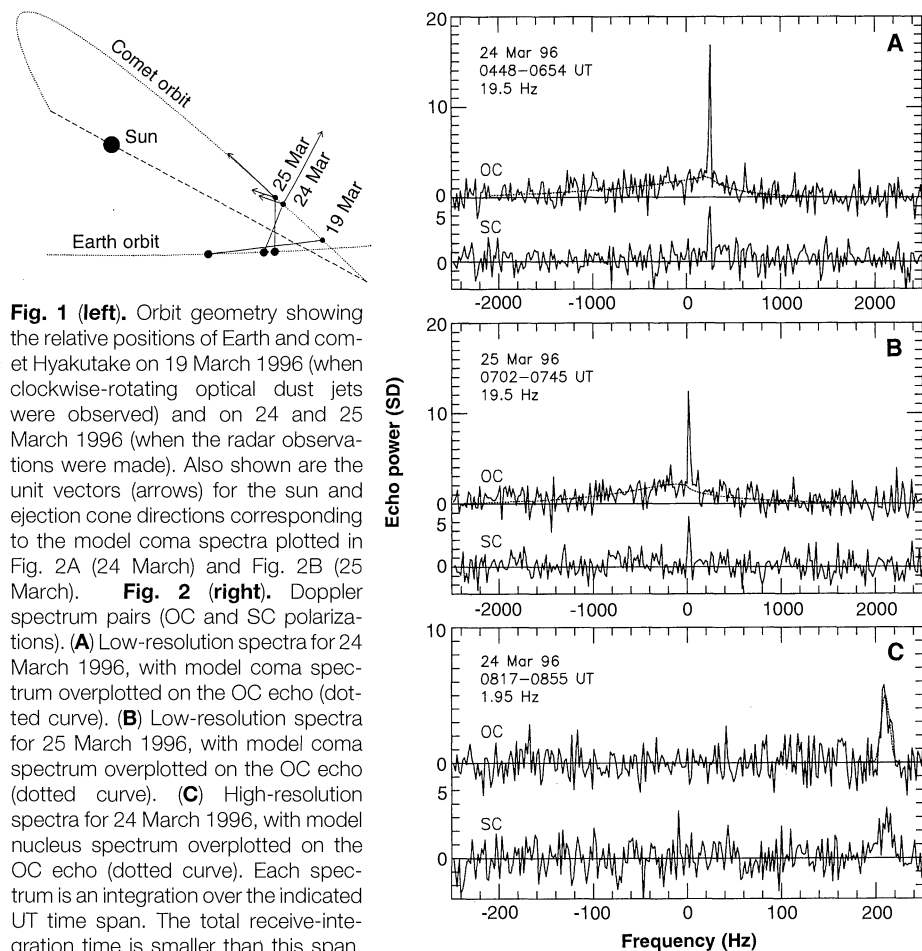


Fig. 1 (left). Orbit geometry showing the relative positions of Earth and comet Hyakutake on 19 March 1996 (when clockwise-rotating optical dust jets were observed) and on 24 and 25 March 1996 (when the radar observations were made). Also shown are the unit vectors (arrows) for the sun and ejection cone directions corresponding to the model coma spectra plotted in Fig. 2A (24 March) and Fig. 2B (25 March). **Fig. 2 (right).** Doppler spectrum pairs (OC and SC polarizations). **(A)** Low-resolution spectra for 24 March 1996, with model coma spectrum overplotted on the OC echo (dotted curve). **(B)** Low-resolution spectra for 25 March 1996, with model coma spectrum overplotted on the OC echo (dotted curve). **(C)** High-resolution spectra for 24 March 1996, with model nucleus spectrum overplotted on the OC echo (dotted curve). Each spectrum is an integration over the indicated UT time span. The total receive-integration time is smaller than this span, and equals 45 min for (A), 18 min for (B), and 15 min for (C). Offsets of the nucleus echo from 0 Hz are caused by errors in the Doppler prediction ephemeris used for the observations. This error also caused the echo to drift across the spectrum at a rate of -15 Hz/hour .

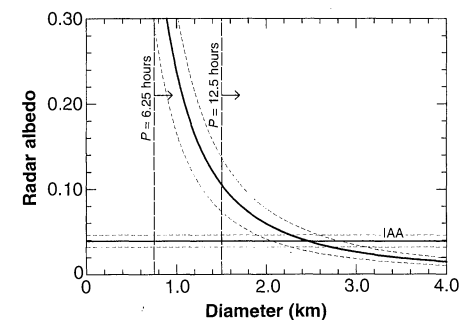


Fig. 3. Radar albedo $4\sigma/\pi D^2$ of the Hyakutake nucleus as a function of nucleus diameter D for an assumed spherical nucleus (solid curve), and the estimated radar albedo of comet IAA (solid horizontal line). The corresponding error bounds (dashed lines) are given for each. Also shown are the lower limits to the nucleus diameter for rotation periods of 6.25 and 12.5 hours.

velocities $V \approx Ca^{-1/2}$ (20). The cone direction and velocity scaling constant C were then free parameters that could be adjusted to match the observed width and offset of the coma echo spectrum. The velocity scaling we used for the model spectra (Fig. 2, A and B) corresponds to an ejection velocity $V = 40$ m/s for 1-cm-radius grains. Our modeling results show that the ejection was not aimed directly at the sun, as this would have offset the coma echo toward positive Doppler shifts. There is a restricted range of directions for which the model spectra match the coma echo reasonably well (21). Examples of model spectra giving good fits are shown in Fig. 2, A and B, and their corresponding direction vectors are shown in Fig. 1. These directions are plausible if the grain ejection is determined by a thermal-phase lag in the solar activation of rotating jets. Observations of optical dust jets around 19 March (22, 23) showed a clockwise rotation, suggesting that, at that time, the nucleus was showing its south pole to Earth (23). This rotation sense is consistent with the comet-sun and ejection-cone vectors in Fig. 1. Because some antisolar directions also give good fits (21), it is possible that there may have been a contribution to the coma echo from the trailing condensation of large grains invoked by Harris *et al.* (24) to explain Hyakutake images obtained on 26 March. Harris *et al.* also argued that evaporation of large icy grains could explain the observed sphericity of the gas coma. Such icy grains, if present, could have contributed to the coma radar echo.

We estimated the grain production rate

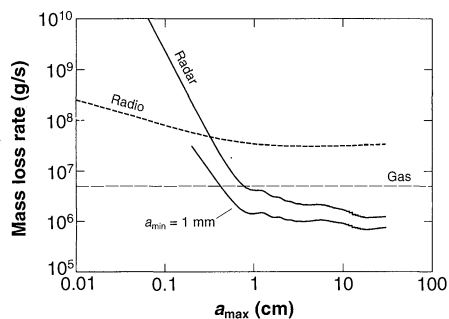


Fig. 4. Mass loss rate \dot{M} in dust and grains as inferred from the radar coma echo (upper solid curve) and from the radio continuum observations (dashed curve) for an $a^{-3.9}$ particle production size distribution with minimum grain size $a_{\min} = 1$ μm and maximum grain size a_{\max} . Also shown is the radar curve corresponding to $a_{\min} = 1$ mm (lower solid curve). The grains were assumed to have a density $\rho = 0.3$ g/cm³ and a complex refractive index $n = 1.25 - i0.01$. The mean gas production rate \dot{M}_g (horizontal dashed line) at the time of the radar observations is shown. Mie theory was used to calculate backscatter efficiencies for the radar curves and absorption efficiencies for the radio curve.

from the strength of the coma echo. We calculated the nucleus mass loss rate \dot{M} (in dust and large grains) from (5) using the velocity scaling from the coma spectrum fits and assuming the grains to have a density (0.3 g/cm³) and refractive index ($n = 1.25$) characteristic of a lightly packed snowball. The grain production size distribution was assumed to be an $a^{-3.9}$ power law between a minimum radius a_{\min} and maximum radius a_{\max} (25). The \dot{M} curve (Fig. 4) shows that the largest grains must exceed 1 mm in radius, or else the grain mass loss rate far exceeds the gas production rate \dot{M}_g , which averaged about 5×10^6 g/s during this period (26). Making the maximum grain size greater than 1 cm gives \dot{M} values that are comparable with the gas production rate and the estimated 5×10^6 g/s dust production rate (15, 26, 27). The radar \dot{M} curve for $a_{\min} = 1$ mm (Fig. 4) shows that the largest grains ($a > 1$ mm) account for about 1×10^6 g/s of the total nucleus mass loss. [This curve is also less sensitive to the assumed power law index than the $a_{\min} = 1$ μm case and gives a good approximation to \dot{M} for the case of a flatter ($a^{-3.5}$) size distribution with $a_{\min} = 1$ μm .] Therefore, the estimated large-grain production rate inferred from the radar cross section of the coma echo is substantial, yet physically reasonable.

The calculated mass loss rates are sensitive to the assumed grain properties. Making the grains solid ice or rock gives \dot{M} values several times smaller than those in Fig. 4, whereas going to lighter grains increases \dot{M} (5). Though these uncertainties in grain density and \dot{M} cannot be resolved from the radar data alone, they can be reduced by comparing the radar results with millimeter-wave radio continuum measurements. In Fig. 4 we show the \dot{M} required to give the continuum flux density of 220 mJy (1 Jy = 10^{-26} W m⁻² Hz⁻¹) measured at $\lambda = 1.1$ mm by Jewitt and Matthews (28); this was calculated with the Rayleigh-Jeans law (5) for a 0.3-g/cm³ dirty snowball ($n = 1.25 - i0.01$). Note that for $a_{\max} > 1$ cm, the radio-derived \dot{M} is an order of magnitude greater than the radar-derived \dot{M} . Calculations showed that this discrepancy cannot be removed by adjusting the size distribution spectral index, nor can the radio \dot{M} curve be lowered much by increasing the grain conductivity (as the large grains are already optically thick). Also, trying silicate grains with densities in the range of 0.5 to 2 g/cm³ made the discrepancy worse regardless of the spectral index. It appears that the only way to reconcile the radar and radio measurements is to invoke grains that are more porous than those we have considered here. Increasing the grain porosity will raise the absorption per unit mass (or "mass opacity" κ) as it lowers the backscatter per unit mass

(29, 30), the combined effect being to bring the radar and radio curves closer to some \dot{M} values intermediate between the curves in Fig. 4. It is known that certain "fluffy" grains can have opacities (at $\lambda = 1$ mm) well in excess of the $\kappa \approx 0.4$ m²/kg that characterizes the radio curve in Fig. 4 (29). Fluffy grains could also help to explain the relatively high velocities that were predicted by our coma spectrum model, because such grains are light and would couple more strongly to the outflowing gas (31).

REFERENCES AND NOTES

1. P. G. Kamoun, D. B. Campbell, S. J. Ostro, G. H. Pettengill, I. I. Shapiro, *Science* **216**, 293 (1982).
2. P. G. D. Kamoun, thesis, Massachusetts Institute of Technology (1983).
3. I. I. Shapiro *et al.*, *Bull. Am. Astron. Soc.* **15**, 800 (1983); J. K. Harmon, unpublished results.
4. R. M. Goldstein, R. F. Jurgens, Z. Sekanina, *Astron. J.* **80**, 1745 (1984).
5. J. K. Harmon, D. B. Campbell, A. A. Hine, I. I. Shapiro, B. G. Marsden, *Astrophys. J.* **338**, 1071 (1989).
6. D. B. Campbell, J. K. Harmon, I. I. Shapiro, *ibid.*, p. 1094.
7. A CW experiment involves transmission of a monochromatic (unmodulated) wave and reception of an echo that has been Doppler-broadened by rotation of the target object. Unlike the CW case, an experiment with a modulated (pulsed or coded) transmission can discriminate in echo delay and hence provide a direct nucleus size estimate if the delay resolution is finer than the nucleus' delay depth.
8. The OC echo is the echo component in the circular polarization sense that is opposite the transmitted sense. This is the expected polarization sense for scattering from smooth surfaces or small particles. The SC echo is the component of the echo received in the same circular polarization sense as the transmitted wave. This echo can be produced by scattering from wavelength-scale surface structure or multiple scattering from a collection of particles.
9. We calibrated the spectrum in the standard fashion, using the system temperature to set the absolute noise background level. The calibrated spectrum gives a radar cross section per frequency bin, although here we display the spectra in units of the noise standard deviation. For the radar cross section we use the standard convention, which references to a perfect isotropic reflector.
10. The quoted errors are two standard deviations. Roughly half the variance is random statistical error and the remainder allows for errors in calibration and pointing.
11. S. J. Ostro *et al.*, *Astron. J.* **102**, 1490 (1991); L. A. M. Benner *et al.*, *Icarus*, in press.
12. E. Kührt, J. Knollenberg, H. U. Keller, *Planet. Space Sci.* **45**, 665 (1997).
13. The smallest radar cross section for a comet is the 0.04 km² value measured for comet Sugano-Saigusa-Fujikawa (3). Infrared observations indicate a diameter of less than 1 km for this comet [M. S. Hanner, R. L. Newburn, H. Spinrad, G. J. Veeder, *Astron. J.* **94**, 1081 (1987)].
14. Z. Sekanina [*ibid.* **95**, 1876 (1988)] estimated the nucleus of comet IAA to have dimensions of 16 km by 7 km and a projected area of 61 km² at the time of the 1983 radar observations. Dividing the IAA radar cross section (4, 5) by this area gives the 0.039 value for the albedo. Of those comet nuclei that have been detected by radar, IAA has the best size estimate, which is the reason we adopt it for our reference albedo.
15. D. G. Schleicher, R. L. Millis, D. J. Osip, S. Lederer, *Bull. Am. Astron. Soc.* **28**, 926 (1996).
16. S. Larson, J. Brandt, C. Randall, M. Niedner, *ibid.*, p. 1088.
17. H. U. Keller *et al.* [*Astron. Astrophys.* **187**, 807 (1987)] estimated dimensions of 15 km by 8 km

for the Halley nucleus.

18. Hyakutake nucleus diameter estimates based on infrared observations are 4.2 ± 0.8 km [J. Sarmecanic, M. Fomenkova, B. Jones, T. Lavezzi, *Astrophys. J.* **483**, L69 (1997)] and 4.8 ± 1.0 km [Y. R. Fernandez *et al.*, *Bull. Am. Astron. Soc.* **28**, 1088 (1996)]. The infrared diameters, if correct, lower the radar albedo to 0.012, implying a surface with the consistency of loosely packed snow. Diameter upper limits based on radio continuum measurements are 5.0 km [I. de Pater *et al.*, *Planet. Space Sci.* **45**, 731 (1997); W. J. Altenhoff *et al.*, *Bull. Am. Astron. Soc.* **28**, 928 (1996)], 6.0 km [Y. R. Fernandez, A. Kundo, C. M. Lisse, M. F. A'Hearn, *Planet. Space Sci.* **45**, 735 (1997)], and 5.7 km (28).
19. D. K. Yeomans, personal communication.
20. The standard model of grain ejection by gas drag (5) gives a terminal grain velocity $V = Ca^{-1/2}g$. The gravity correction $g = (1 - a/a_m)^{1/2}$ is a function of the maximum liftable grain radius $a_m = 9V_g\dot{\mu}/16\pi\rho_n\rho G$, where V_g and $\dot{\mu}$ are the gas velocity and gas mass flux at the surface, R is nucleus radius, ρ_n and ρ are the nucleus and grain densities, and G is the gravitational constant.
21. A survey of all ejection directions shows a locus of directions giving fits with χ^2_ν better than 1.08. These include some antisolar directions, some directions opposite the orbital angular momentum vector, and a band that crosses the comet orbit plane at an azimuth angle of -40° to the sun direction.
22. R. M. West, *Int. Astron. Union Circ.* 6343 (1996).
23. L. Jorda, J. Lecacheux, F. Colas, *Int. Astron. Union Circ.* 6344 (1996).
24. W. M. Harris, M. R. Combi, R. K. Honeycutt, B. E. A. Mueller, F. Scherb, *Science* **277**, 676 (1997).
25. Here a_{\max} is a simple size distribution cutoff introduced to show the sensitivity of M to maximum grain size. We chose to use this cutoff parameter instead of the maximum liftable grain radius, a_m (5, 20), because varying a_m implies varying the grain velocity, whereas here we hold the velocity scaling C at a fixed value determined from the coma spectrum fits. For this comet, a_m is likely to be very large (~ 10 m).
26. D. Schleicher, *Int. Astron. Union Circ.* 6372 (1996); M. J. Mumma, M. A. Di Santi, N. Dello Russo, D. X. Xie, *Int. Astron. Union Circ.* 6366 (1996).
27. J. Sarmecanic, M. Fomenkova, B. Jones, *Bull. Am. Astron. Soc.* **28**, 1089 (1996).
28. D. C. Jewitt and H. E. Matthews, *Astron. J.* **113**, 1145 (1997).
29. E. L. Wright, *Astrophys. J.* **346**, L89 (1989); D. C. Jewitt and J. X. Luu, *Icarus* **100**, 187 (1992).
30. J. I. Hage and J. M. Greenberg, *Astrophys. J.* **361**, 251 (1990).
31. In the standard model (20) the velocity scaling constant $C = (3C_D C_E V_g \dot{\mu} R/4\rho)^{1/2}$, where C_D is a drag coefficient and C_E corrects for the change in V_g with expansion. To get $V = 40$ m/s for homogeneous spherical grains ($C_D = 2$, $C_E \approx 9/4$) of 0.3 g/cm³ density and 1-cm radius requires a gas flux of $\dot{\mu} = 4 \times 10^{-4}$ g/cm²-s for $V_g = 0.29$ km/s (300 K gas). This is higher than the $\dot{\mu} = 5 \times 10^{-5}$ g/cm²-s that one expects from steady sublimation of a clean ice surface. Making the grains fluffy or fractal can ease the requirement of a high $\dot{\mu}$ because of the lower density ρ and higher drag coefficient C_D [H. U. Keller and W. J. Markiewicz, *Geophys. Res. Lett.* **18**, 249 (1991)]. However, $\dot{\mu}$ could also be higher than the steady sublimation value if the gas release is explosive or jetlike.
32. We thank the AlliedSignal Technical Support Corporation personnel who operate the antennas and support facilities at the Goldstone Deep Space Communications Complex under contract with the Jet Propulsion Laboratory. L.A.M.B. was supported as a research associate of the National Research Council. Part of this research was conducted at the Jet Propulsion Laboratory, California Institute of Technology, under contract with NASA. The remainder of the work was done at the National Astronomy and Ionosphere Center (Arecibo Observatory), which is operated by Cornell University under a cooperative agreement with NSF and with support from NASA.

19 August 1997; accepted 28 October 1997

Spontaneous Formation of Macroscopic Chiral Domains in a Fluid Smectic Phase of Achiral Molecules

Darren R. Link, Giorgio Natale, Renfan Shao, Joseph E. Maclennan, Noel A. Clark, Eva Körblová, David M. Walba

A smectic liquid-crystal phase made from achiral molecules with bent cores was found to have fluid layers that exhibit two spontaneous symmetry-breaking instabilities: polar molecular orientational ordering about the layer normal and molecular tilt. These instabilities combine to form a chiral layer structure with a handedness that depends on the sign of the tilt. The bulk states are either antiferroelectric-racemic, with the layer polar direction and handedness alternating in sign from layer to layer, or antiferroelectric-chiral, which is of uniform layer handedness. Both states exhibit an electric field-induced transition from antiferroelectric to ferroelectric.

Chirality has been recognized as an important feature of liquid crystals (LCs) since the time of their discovery (1). Now the influence of chirality on phase behavior and macroscopic structure is of major interest in LC science, stimulated in part by the recent discoveries of the blue phases (2) and of chiral smectic (Sm) ferroelectric (3), antiferroelectric (4), and twist grain boundary (5) phases. In these and all other known chiral LC phases, the chirality is of molecular origin, being built into the molecular structure upon synthesis, and is essentially permanent. Here we report macroscopically chiral LC phases obtained by the spontaneous chiral organization of achiral molecules. Specifically, we have found coexisting bulk fluid chiral Sm domains of opposite handedness spontaneously formed from molecules that are achiral in the isotropic phase. We provide evidence for the spontaneous formation of chiral layers in a Sm phase made from achiral molecules with bent cores [the homologous compounds 1 (6) and 2 (7) (Fig. 1)] and provide structural evidence for a symmetry-breaking transition to polar ordering in an achiral LC.

The current interest in the LC behavior of bent-core molecules has been stimulated by the synthetic work of Matsunaga and colleagues (7, 8), which includes the design and synthesis of compound 2 and its homologs (7). They identified the highest temperature Sm phase in 2 as a smectic C (SmC) and used x-ray layer spacing measurements of the homologous series to argue that the tails are nearly normal to the Sm layers whereas the cores are tilted. They found an 18.5 Å core thickness and, assuming a core conformation

giving a 27.5 Å spacing between the alkoxy oxygens of 2, obtained a core tilt of 48° (7). Recently, Watanabe, Takezoe, and co-workers (6) synthesized and studied the alkyl homologs of compound 1, concluding from optical measurements that its highest temperature Sm phase had untilted cores and, from switching current measurements, that there was ferroelectric ordering of the molecular bows, with their arrows pointing in a particular direction that could be switched by an applied electric field. Study by Weissflog *et al.* (9) of the octyl homolog of 2 showed an antiferroelectric current response and led them to a model with an untilted core structure and antiferroelectric ordering of the molecular bows. Heppke *et al.* observed ferroelectric switching current dynamics in several other homologs of 1 and 2 (10).

Here we present the results of optical microscopy studies of the highest temperature Sm phase of compounds 1 and 2 in the freely suspended film (11) and "bookshelf" (12) electro-optical geometries. Our work, directed toward revealing the structure of this phase, demonstrates (i) the layer-by-layer antiferroelectric structure of the equilibrium phase, (ii) spontaneous breaking of achiral symmetry in a bulk LC (in this case into chiral Sm layers), (iii) the existence of racemic (R) and homogeneously chiral (H) stacking of these chiral layers, the racemic being the lower free-energy state, (iv) the coexistence of macroscopic, homogeneously chiral domains of opposite handedness, which maintain their handedness during electro-optic switching and are identifiable by their chiral response to applied electric field, and (v) "sergeants-and-soldiers" biasing of the global chirality by addition of chiral dopant. On the basis of these observations, we have adopted the nomenclature "SmCP_A" for this phase (13). The SmCP_A phase of both compounds 1 and 2 behaved in essentially identical fashion in the film and

D. R. Link, G. Natale, R. Shao, J. E. Maclennan, N. A. Clark, Department of Physics, Condensed Matter Laboratory, University of Colorado, Boulder, CO 80309, USA. E. Körblová and D. M. Walba, Department of Chemistry and Biochemistry, University of Colorado, Boulder, CO 80309, USA.